Chromatic Dispersion Compensation in Phase-Stabilized Dissemination System of Broadband Signals Based on Phase Conjugation

Tao Wang, Yi Liu, Kaiyu Zhang, Zhengyang Xie, Shangyuan Li, Dong Wang, and Zheng Zheng, *Member, IEEE*

***Abstract*—We present a dispersion-independent phase stabilized distribution architecture for broadband signal based on photonic microwave phase conjugation. RoF signals are distributed from the central station to each base station via a fiber ring network. The elimination of dispersion-induced optical phase decorrelation is achieved because the backward transmission of the phase-conjugated signal, thus the EVM of the RoF signal is optimized. A proof-of-concept experiment is demonstrated. A distribution of QPSK modulated 23-GHz, 400M Baud RoF signals from the central station to a remote base station is obtained via a fiber optic loop. The demodulated constellation and error vector magnitude with and without dispersion compensation are measured at the remote base station. When we set the length of the fiber loop to 58 km, the EVM is reduced by 8% after dispersion compensation, and the compensated EVM can reach the threshold value of 17.5% specified by 3 GPP for 5G when the received optical power of PD is 4 dBm.**

***Index Terms*—Optical phase decorrelation, photonic microwave phase conjugation, radio over fiber, chromatic dispersion.**

I. Introduction

PHASE-STABILIZED transmission of radio frequency (RF) signals in distributed antenna system has received a lot of attention due to its important applications in many fields, such as distributed synthetic aperture radar, deep space network detection, navigation and positioning, and precision measurements [1], [2], [3], [4]. Considering weight and cost, remote distribution of stable radio frequency (RF) signal along optical fibers is advantageous [5]. Fiber-based frequency synchronization has been under extensive research, and it achieves high precision frequency synchronization by compensating phase fluctuation in real time. However, most studies have focused on phase fluctuation caused by temperature drift and mechanical vibration in the environment where the fiber is located [6], [7]. In addition, phase decorrelation due to fiber dispersion will become important after long-distance transmission, especially when using lasers with wide linewidths, because dispersion introduces different delays in different optical tones [8]. In the last few years, several studies on compensating chromatic dispersion to improve the signal quality have been reported and can be divided into two categories. One is hardware-based techniques, such as spectral processing-based phase adjustment techniques, which can effectively eliminate the delay difference due to dispersion, but are limited by the response speed of the spectral processor [9]. Another approach is algorithm-based, using stochastic theory to calculate and compensate the deterioration caused by the de-correlated phase jitter term [10], [11]. However, with further deterioration in noise level, the huge computational effort makes it impossible to guarantee the feasibility of applying real-time demodulating.

Moreover, previous methods are usually designed for the propagation of monophonic signals, and a new stable phase transmission scheme for broadband signals is proposed in [12], however, the bandwidth is limited because it does not involve microwave photonic frequency multiplication techniques. The generation of photonic vector RF signal based on frequency multiplication has been extensively studied, not only because of its huge bandwidth, but also because it is effectively compatible with radio-over-fiber systems [13]. There are two main methods of photonic vector RF signal generation. One is the use of precoding-assisted techniques at the transmitter [14], [15]. However, for higher order modulation formats, the system performance will deteriorate. The other is based on single sideband (SSB) modulation to generate millimeter waves, which avoids precoding and thus improves spectral efficiency [16], [17]. In addition, single sideband avoids the periodic fading of power introduced by dispersion.

We propose a dispersion-independent distributed antenna system for stable distribution of the broadband signals based on phase conjugation, in which different delays in optical tones

Manuscript received 20 May 2023; revised 8 July 2023; accepted 24 August 2023. Date of publication 28 August 2023; date of current version 4 September 2023. This work was supported in part by the National Key Research and Development Program of China under Grant 2021YFB2800605, in part by the Fundamental Research Funds for the Central Universities under Grant 2242022k60006, and in part by the National Natural Science Foundation of China (NSFC) under Grants 61901026 and 62175054. *(Corresponding author: Zhengyang Xie.)*

Tao Wang, Yi Liu, Kaiyu Zhang, Zhengyang Xie, and Zheng Zheng are with the Department of Electronic Engineering, Beihang University, Beijing 100191, China (e-mail: wtzy2102405@buaa.edu.cn; eeleahliu@buaa.edu.cn; zkyvan@buaa.edu.cn; xiezy@buaa.edu.cn; zhengzheng@buaa.edu.cn).

Shangyuan Li is with the Beijing National Research Center for Information Science and Technology, Department of Electronic Engineering, Tsinghua University, Beijing 100084, China (e-mail: syli@mail.tsinghua.edu.cn).

Dong Wang is with the Department of Fundamental Network Technology, China Mobile Research Institute, Beijing 100053, China (e-mail: wangdongyjy @chinamobile.com).

Digital Object Identifier 10.1109/JPHOT.2023.3309313

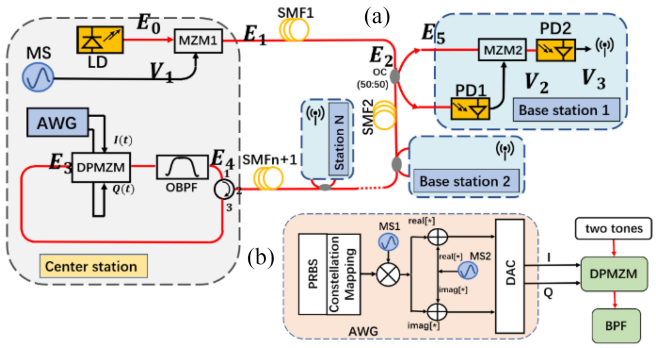

Fig. 1. (a) The schematic diagram of the proposed vector signal transmission system. (b) The schematic diagram of the proposed SSB vector signal generation system.

due to dispersion is automatically eliminated. This structure has better adaptability compared to active dispersion compensation devices and receiver-side algorithms for dispersion compensation, which are not limited by response speed or computational effort. The phase conjugator at the central station also helps to generate SSB vector signals, simplifying the architecture of remote base stations. An automatic cancellation of the time delay difference is deployed to compensate the dispersion and improve the signal quality. This process is implemented because the phase-conjugated signal undergoes reverse transmission and photonic microwave mixing operations at each remote station. We perform a proof-of-concept experiment to implement the distribution of a vector signal with modulation format QPSK, code rate 400M, and frequency 23 GHz in a fiber optic loop system consisting of SMF1 and SMF2. We adjust the loop length to explore the compensation performance. When we fix the length of SMF2 to 8 km and adjust SMF1 to 50 km, the EVM of the compensated signal still meets the threshold of 17.5% specified by 3GPP for 5G. And in this case, the EVM can be reduced by 8% after compensation.

II. System Architecture and Operation Principle

The schematic diagram of the dispersion-independent distributed antenna system based on the photonic microwave phase conjugation is shown in Fig. 1(a). The central station is connected to each remote base station with a fiber optic loop. Broadband RF signals are generated remotely in each base station unit. If there are N remote base stations, the fiber loop will consist of N+1 single-mode fibers (SMF). For simplicity, we will analyze the case of only one remote antenna unit, however, the corresponding principles apply to any remote base station with the same configuration. In our previous studies, it has been shown that a similar structure can suppress phase fluctuation caused by fiber temperature drift and achieve stable transmission of a single frequency [18], [19]. In this paper, we derive in detail the process of automatic elimination of dispersion and explain the structural principles of vector signal generation without precoding modulation verification.

It is assumed that both the optical carrier wave from the laser diode (LD) and the electrical drive signal from the microwave source (MS) are essentially continuous waves (CW). Therefore, they can be expressed as

$$E_o \propto \cos\left[\omega_o t + \varphi_o(t)\right] \tag{1}$$

and

$$V_1 \propto \cos\left[\omega_e t + \varphi_e(t)\right] \tag{2}$$

where ω_o and ω_e are the angular frequencies of the optical carrier and electrical drive signal, respectively, $\varphi_o(t)$ and $\varphi_e(t)$ are two independent random processes that introduce phase fluctuations into the optical and electrical signals, respectively. Because phase noise dominates our research, the amplitude and intensity noise can be ignored.

The Mach Zehnder modulator (MZM1) is biased at its null point to get the carrier suppression double sideband (CS-DSB) signal. Then the output of the modulator is approximately an optical dual tone signal, E_1, which can be expressed as

$$E_1 \propto \left\{ \begin{array}{l} \cos\left[\left(\omega_o - \omega_e\right)t + \varphi_o\left(t\right) - \varphi_e\left(t\right)\right] \\ \quad + \cos\left[\left(\omega_o + \omega_e\right)t + \varphi_o\left(t\right) + \varphi_e\left(t\right)\right] \end{array} \right\} \tag{3}$$

It is worth noting that the phase noise of the dual tone signal is completely correlated. However, when transmitting through SMF1, different time delays will be introduced to both sidebands due to dispersion. The delay difference between the first order sideband and the optical carrier is given by the following equation [20]

$$\tau_{d1} = \frac{DL_1\lambda_o^2 f_e}{c} \tag{4}$$

where D is the dispersion parameter of the optical fiber, L_1 is the length of the SMF1, λ_o is the central wavelength of the optical carrier, f_e is the frequency of the electrical drive signal, and c is the speed of light in free space.

Therefore, at the end of SMF1, the expression of the optical signal is

$$E_2 \propto \left\{ \begin{array}{l} \cos\left[\begin{array}{l}\left(\omega_o - \omega_e\right)\left(t - \tau_{d1}\right) \\ \quad + \varphi_o\left(t - \tau_{d1}\right) - \varphi_e\left(t - \tau_{d1}\right)\end{array}\right] \\ \quad + \cos\left[\begin{array}{l}\left(\omega_o + \omega_e\right)\left(t + \tau_{d1}\right) \\ \quad + \varphi_o\left(t + \tau_{d1}\right) + \varphi_e\left(t + \tau_{d1}\right)\end{array}\right] \end{array} \right\} \tag{5}$$

Similarly, when transmitted back to the central station through SMF2, the optical signal expression is

$$E_3 \propto \left\{ \begin{array}{l} \cos\left[\begin{array}{l}\left(\omega_o - \omega_e\right)\left(t - \tau_d\right) \\ \quad + \varphi_o\left(t - \tau_d\right) - \varphi_e\left(t - \tau_d\right)\end{array}\right] \\ \quad + \cos\left[\begin{array}{l}\left(\omega_o + \omega_e\right)\left(t + \tau_d\right) \\ \quad + \varphi_o\left(t + \tau_d\right) + \varphi_e\left(t + \tau_d\right)\end{array}\right] \end{array} \right\} \tag{6}$$

where, τ_d is the total loop delay difference, $\tau_d = \tau_{d1} + \tau_{d2}$. Similar to (4), τ_{d2} is the time delay difference caused by dispersion when passing through SMF2.

The arbitrary wave generator (AWG) is used to generate the RF SSB signal. The generation principle is shown in Fig. 1(b). A pseudo-random binary sequence (PRBS) with a certain length is fed to the constellation mapping module. The constellation mapping module is responsible for generating the SSB baseband signal. Subsequently, the SSB baseband signal is upconverted to

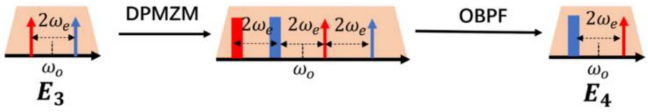

Fig. 2. Spectrum of the photonic-microwave phase conjugation and SSB-RoF signal generation.

a RF SSB signal by mixing with a complex sinusoidal source with an angular frequency of $-2\omega_e$ from the MS1. The real and imaginary parts of the RF SSB signal are then summed with the real and imaginary parts of another complex sinusoidal RF source with a frequency of $2\omega_e$ from the MS2 as the in-phase and quadrature components of the signal, respectively. The IQ data is then uploaded to a digital-to-analog converter (DAC). Then, the I and Q signals output from the DAC are used to drive the I and Q ports of the dual parallel modulator (DPMZM), respectively. The I/Q modulator is operated at the quadrature point and both MZMs in the embedded modulator are operated at the null point [21]. Next, the spectrum evolution of the modulation process is shown in Fig. 2. The I and Q signals generated by the AWG modulate the optical signals E_3 at frequencies of $\omega_o - \omega_e$ (red) and $\omega_o + \omega_e$ (blue), and then generate their own CS-SSB RoF signals (with the same color as them in Fig. 2). Since the frequency interval between the two optical carriers is $2\omega_e$, which is equal to the frequency of the IQ signal, the two intermediate first-order optical sidebands achieve phase switching, and then the other two first-order OSBs are filtered out by an optical bandpass filter (OBPF). The output optical signal is expressed as:

$$E_4 \propto \left\{ \begin{array}{l} \cos\left[\begin{array}{c} (\omega_o+\omega_e)(t-\tau_d)+2\omega_e\tau_d \\ +2\varphi_e(t)+\varphi_o(t-\tau_d)-\varphi_e(t-\tau_d) \end{array} \right] \\ \quad +\left\{ \cos\frac{\pi[V_\pi+I(t)]}{2V_\pi}+\mathrm{j}\cdot\cos\frac{\pi[V_\pi+Q(t)]}{2V_\pi} \right\} \\ \cdot\cos\left[\begin{array}{c} (\omega_o-\omega_e)(t+2\tau_d)+2\omega_e\tau_d \\ -2\varphi_e(t)+\varphi_o(t+\tau_d)+\varphi_e(t+\tau_d) \end{array} \right] \end{array} \right\} \tag{7}$$

The phase conjugation signal E_4 propagates backward along SMF2 to the base station. Due to the same fiber length (including length fluctuations due to environmental changes), forward and backward signals transmitted through SMF2 will experience the same dispersion delay difference loss τ_{d2}. Therefore, E_5 extracted from the reverse signal through OC can be written as

$$E_5 \propto \left\{ \begin{array}{l} \cos\left[\begin{array}{c} (\omega_o+\omega_e)(t-\tau_d+\tau_{d2}) \\ +2\omega_e\tau_d+2\varphi_e(t+\tau_{d2}) \\ +\varphi_o(t-\tau_d+\tau_{d2})-\varphi_e(t-\tau_d+\tau_{d2}) \end{array} \right] \\ \quad +\left\{ \cos\frac{\pi[V_\pi+I(t)]}{2V_\pi}+\mathrm{j}\cdot\cos\frac{\pi[V_\pi+Q(t)]}{2V_\pi} \right\} \\ \cdot\cos\left[\begin{array}{c} (\omega_o-\omega_e)(t+\tau_d-\tau_{d2}) \\ +2\omega_e\tau_d+2\varphi_e(t-\tau_{d2}) \\ +\varphi_o(t+\tau_d-\tau_{d2})+\varphi_e(t+\tau_d-\tau_{d2}) \end{array} \right] \end{array} \right\} \tag{8}$$

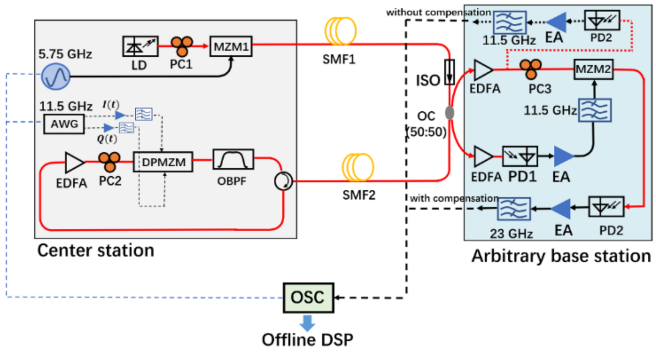

Fig. 3. Experiment setup of vector signal distribution system. LD: Laser diode. PC: Polarization controller. MZM: Mach-Zehnder modulator. SMF: Single mode fiber. EDFA: Erbium-doped fiber amplifier. DPMZM: Dual-parallel Mach-Zehnder modulator. OBPF: Optical bandpass filter. PD: Photodetector. EA: Electric amplifier. OC: Optical coupler. ISO: Isolator. OSC: Digital oscilloscope.

Due to $\tau_d = \tau_{d1} + \tau_{d2}$, (8) can be simplified as

$$E_5 \propto \left\{ \begin{array}{l} \cos\left[\begin{array}{c} (\omega_o+\omega_e)(t-\tau_{d1})+2\omega_e\tau_d+2\varphi_e(t+\tau_{d2}) \\ +\varphi_o(t-\tau_{d1})-\varphi_e(t-\tau_{d1}) \end{array} \right] \\ \quad +\left\{ \cos\frac{\pi[V_\pi+I(t)]}{2V_\pi}+\mathrm{j}\cdot\cos\frac{\pi[V_\pi+Q(t)]}{2V_\pi} \right\} \\ \cdot\cos\left[\begin{array}{c} (\omega_o-\omega_e)(t+\tau_{d1})+2\omega_e\tau_d+2\varphi_e(t-\tau_{d2}) \\ +\varphi_o(t+\tau_{d1})+\varphi_e(t+\tau_{d1}) \end{array} \right] \end{array} \right\} \tag{9}$$

The optical coupler (OC) extracts E_2 from the forward signal, and then passes through a photodetector (PD1) to obtain the RF signal carrying the dispersion in SMF1, which is represented as

$$V_2 \propto \cos\left[\begin{array}{c} 2\omega_e t+2\omega_o\tau_{d1}+\varphi_e(t+\tau_{d1})+\varphi_e(t-\tau_{d1}) \\ +\varphi_o(t+\tau_{d1})-\varphi_o(t-\tau_{d1}) \end{array} \right] \tag{10}$$

In MZM2, V_2 modulates the phase conjugated signal E_5. After the optical mixing at PD2, the phase of V_2 is canceled out by the reverse phase term of the electrical signal in E_5. Therefore, the fourth harmonic term in the mixed product is filtered out by an electrically bandpass filter (EBPF), denoted as

$$\begin{aligned} V_3 \propto & \left\{ \cos\frac{\pi[V_\pi+I(t)]}{2V_\pi}+\mathrm{j}\cdot\cos\frac{\pi[V_\pi+Q(t)]}{2V_\pi} \right\} \\ & \cdot\cos\left[4\omega_e t+2\varphi_e(t+\tau_{d2})-2\varphi_e(t-\tau_{d2})\right] \end{aligned} \tag{11}$$

There is no item like φ_o(t) in V_3 which is related to the phase noise of the LD, so the decorrelation caused by the chromatic dispersion have been automatically removed. Note that in PD1 and PD2, the phases of the vector signals are not doubled when beating to generate the RF signals, which means that precoding operation is not required.

III. Experiment and Results

The experimental setup is based on the configuration in Fig. 3. RoF signals are transmitted in a ring network through non-dispersion shifted fibers (G652D), which is suitable for metropolitan area networks. An isolator (ISO) is connected after SMF1 to avoid backward light return to the central station. At the central station, a distributed feedback laser (DFB) with a

linewidth of 10 MHz is used and its wavelength is set to 1550.0 nm to ensure minimal attenuation in the fiber loop. The wide linewidth of the laser makes the de-correlation introduced by dispersion obvious. The MZM1 (Fujitsu FTM7920) is used to modulate a 5.75-GHz LO reference, and DPMZM (Fujitsu FTM7961EX) is used as a tool for phase conjugation and single-sideband modulation. To reduce the interference from the backward optical signal, a circulator with the isolation of 60 dB is used. A PRBS with the length of (2^{14}) is mapped to QPSK and then converted to an 11.5 GHz SSB signal with a bandwidth of 400 MHz in the AWG (Tektronix AWG70002A), which uses the same clock reference as the LO. The IQ outputs of the AWG are then amplified equally by two identical electronic amplifiers (SHWLNA-0618-29P7S) to drive the DPMZM. The remote station consists of PD, BPF, EDFA, MZM and EA. The MZM2(Fujitsu FTM7920) is used for photonic microwave mixing. Two 43 Gb/s photodetectors (Finisar MPRV1331A) have consistent detection characteristics. Two electrical bandpass filters (BPF) with the same bandwidth of 600 MHz are focused at 11.5 GHz and 23 GHz, respectively. They are used to filter out the required signals. In addition, polarization controllers PC1, PC2, and PC3 are added in front of all modulators in the system in order to reduce polarization losses.

To demodulate and recover the original data, we use a digital oscilloscope (OSC, Keysight UXR0134A) with the sampling rate of 40G to sample the data for offline DSP processing. The sampled data then are upload to the computer for demodulation processing which includes down conversion, constant modulus algorithm (CMA), frequency offset estimation (FOE), carrier phase recovery (CPR). constellation plotting and error vector magnitude (EVM) calculating. In order to evaluate the compensation performance of the system at different fiber dispersion levels, the length of SMF1 is set to 25 km, 50 km and 80 km, and the length of SMF2 is kept at 8 km. Fig. 4 shows the constellation of compensated and uncompensated QPSK signals with different lengths of SMF1. Observing Fig. 4(a), (c) and (e), the effect of the de-correlation caused by dispersion becomes obvious as the transmission length increases. By comparing Fig. 4(a) with (b), (c) with (d) and (e) with (f), it shows that the dispersion compensation makes the points in the constellation more concentrated.

Fig. 5 records the correlation between the EVM of the signal and the SMF1 whose distance is swept by 2 km per step. For G652D fiber, the corresponding dispersion is 34ps/nm. The results show that the compensation performance of the system becomes more effective as the dispersion increases. It is worth noting that the EVM of the compensated signal (the green line in Fig. 5) still deteriorates as the transmission distance increases. This is due to the degradation of signal-to-noise ratio (SNR) caused by signal attenuation and ASE of the EDFAs. The EVM of remote transmission can be optimized by adding optical filters after EDFAs to improve the SNR.

Fig. 6 shows the EVM versus received optical power for the transmission of a QPSK signal at 400M Baud under different scenarios. Due to the limitations of the PD device used in the experiment, the maximum received optical power we measured is 4 dBm.When the SMF1 length is set to 10 km, the curves with

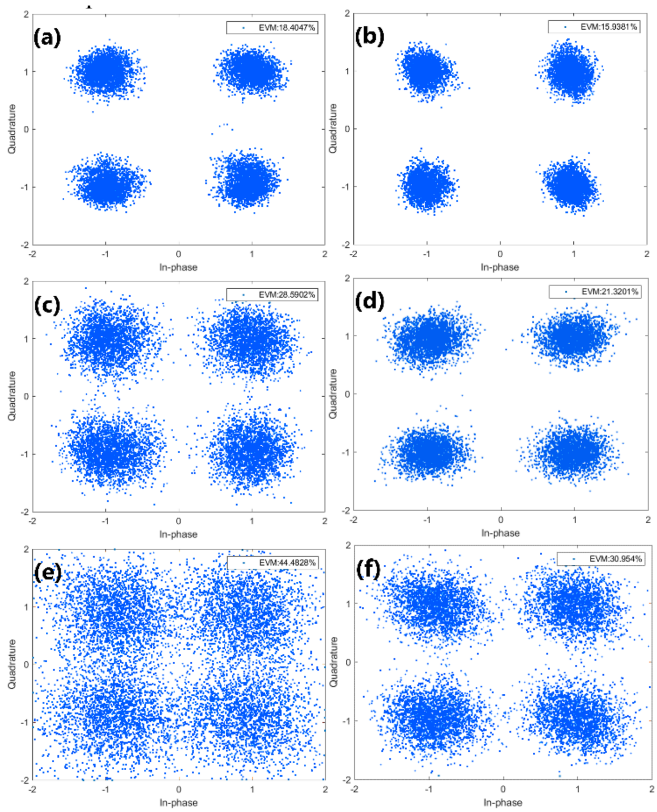

Fig. 4. Demodulation constellation with different lengths of SMF1 with and without compensation. (a) 25 km without compensation (EVM = 18.4%). (b) 25 km with compensation (EVM = 15.9%). (c) 50 km without compensation (EVM = 28.5%). (d) 50 km with compensation (EVM = 21.3%). (e) 80 km without compensation (EVM = 44.5%). (f) 80 km with compensation (EVM = 30.9%).

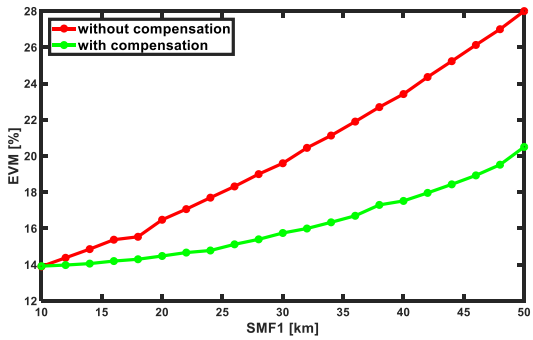

Fig. 5. EVM of the with and without compensation vector signals as a function of the length of SMF1.

and without compensation approximately overlap, as shown in Fig. 6(a), with a 1 dB power penalty compared to the BTB transmission. The power penalty of the signal with compensation in Fig. 6(b), (c), (d) and (e) are 1.3 dB, 5 dB, 10 dB and 12 dB at 17.5% EVM compared to BTB. As shown in Fig. 6(b), when set to 20 km, the EVM with compensation can be kept within the range of 17.5% specified by 3GPP at a received optical power of −9.7 dBm, while the EVM value without compensation can be kept within 17.5% at the received optical power of −7 dBm.

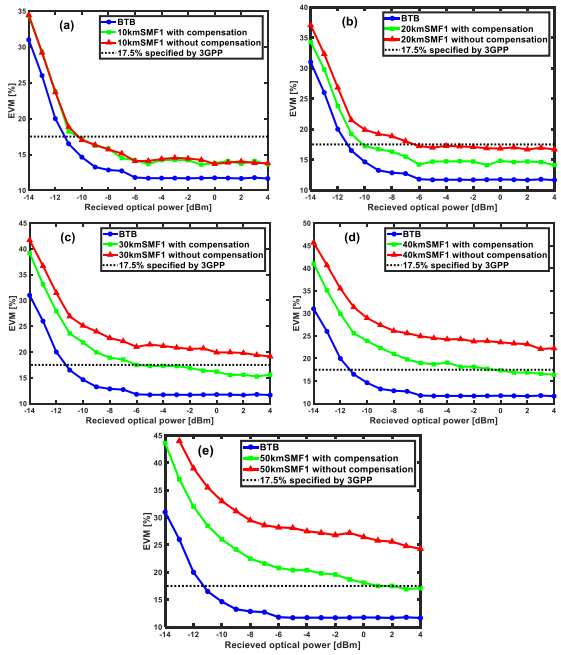

Fig. 6. Measured EVM results versus received optical power for signals with and without compensation at different transmissions. (a) 10 km SMF1. (b) 20 km SMF1. (c) 30 km SMF1. (d) 40 km SMF1. (e) 50 km SMF1.

Therefore, the dispersion compensation increases the receiver sensitivity by 2.7 dB. As shown in Fig. 6(c)–(e), the receiver sensitivity of the compensation signal is −6 dBm, −2 dBm and 1 dBm when the SMF1 is 30 km, 40 km and 50 km. However, in all three cases, the EVM of the uncompensated signal cannot reach the threshold of 17.5%, which reflects the necessity of the dispersion compensation. Furthermore, in Fig. 6(a)–(e), the average EVM of the compensated signals can be stabilized at 14.11%, 14.36%, 15.71%, 16.65% and 17.48% within the threshold specified by 3GPP for 5G, respectively.

IV. Conclusion

In summary, we propose an automatic compensation system for decorrelation induced by dispersion. This structure is applicable to the distribution system for phase-stabilized distribution of broadband signals. We successfully demonstrate the distribution of 23 GHz vector RoF signal with a bandwidth of 400 MHz from the central station to the remote base station in this structure. And the compensation performance of the structure for the RoF vector signal was compared under different fiber lengths and received optical powers. The results show that the suppression of dispersion becomes obvious with the increase of length of fiber. After 58 km transmission, the EVM decreases by 8%. The signal after compensation can reach the EVM standard of 17.5% specified by 3GPP at a received optical power of 4 dBm.

References

[1] W.-Q. Wang, "GPS-based time & phase synchronization processing for distributed SAR," *IEEE Trans. Aerosp. Electron. Syst.*, vol. 45, no. 3, pp. 1040–1051, Jul. 2009.

[2] M. Calhoun, S. Huang, and R. L. Tjoelker, "Stable photonic links for frequency and time transfer in the deep-space network and antenna arrays," *Proc. IEEE*, vol. 95, no. 10, pp. 1931–1946, Oct. 2007.

[3] P. Ghelfi et al., "Photonics in radar systems: RF integration for state-of-the-art functionality," *IEEE Microw. Mag.*, vol. 16, no. 8, pp. 74–83, Sep. 2015.

[4] J.-F. Cliche and B. Shillue, "Applications of control precision timing control for radioastronomy maintaining femtosecond synchronization in the Atacama large millimeter array," *IEEE Control Syst.*, vol. 26, no. 1, pp. 19–26, Feb. 2006.

[5] A. Moerman et al., "Beyond 5G without obstacles: mmWave-over-fiber distributed antenna systems," *IEEE Commun. Mag.*, vol. 60, no. 1, pp. 27–33, Jan. 2022.

[6] M. Jiang et al., "Multi-access RF frequency dissemination based on round-trip three-wavelength optical compensation technique over fiber-optic link," *IEEE Photon. J.*, vol. 11, no. 3, Jun. 2019, Art. no. 7202808.

[7] R. Wu, J. Lin, T. Jiang, C. Liu, and S. Yu, "Stable radio frequency transfer over fiber based on microwave photonic phase shifter," *Opt. Exp.*, vol. 27, no. 26, 2019, Art. no. 38109.

[8] C.-C. Wei, C.-T. Lin, M.-I. Chao, and W.-J. Jiang, "Adaptively modulated OFDM ROF signals at 60 GHz over long-reach 100-km transmission systems employing phase noise suppression," *IEEE Photon. Technol. Lett.*, vol. 24, no. 1, pp. 49–51, Jan. 2012.

[9] L. Li et al., "Suppression for dispersion induced phase noise of an optically generated millimeter wave employing optical spectrum processing," *Opt. Lett.*, vol. 37, no. 19, 2012, Art. no. 3987.

[10] J. P. Santacruz, S. Rommel, U. Johannsen, A. Jurado-Navas, and I. T. Monroy, "Analysis and compensation of phase noise in mm-Wave OFDM AROF systems for beyond 5G," *J. Lightw. Technol.*, vol. 39, no. 6, pp. 1602–1610, 2021.

[11] H.-T. Huang, W.-L. Liang, C.-C. Wei, C.-T. Lin, and S. Chi, "150-km 103-GHz direct-detection OFDM-ROF system employing pilot-aided phase noise suppression," in *Proc. Opt. Fiber Commun. Conf.*, 2014, pp. M2D–M26.

[12] J. Qiu, Z. Li, X. Jin, X. Yu, S. Zheng, and X. Zhang, "Long distance broadband fiber optical beamforming over 120 km," *IEEE Access*, vol. 9, pp. 152182–152187, 2021.

[13] X. Li, J. Zhang, J. Xiao, Z. Zhang, Y. Xu, and J. Yu, "W-band 8QAM vector signal generation by MZM-based photonic frequency octupling," *IEEE Photon. Technol. Lett.*, vol. 27, no. 12, pp. 1257–1260, Jun. 2015.

[14] X. Li et al., "QAM vector signal generation by optical carrier suppression and precoding techniques," *IEEE Photon. Technol. Lett.*, vol. 27, no. 18, pp. 1977–1980, Sep. 2015.

[15] Y. Wang, C. Yang, N. Chi, and J. Yu, "Photonic frequency-quadrupling and balanced pre-coding technologies for W-band QPSK vector mm-Wave signal generation based on a single DML," *Opt. Commun.*, vol. 367, pp. 239–243, 2016.

[16] W. Zhou, L. Zhao, J. Zhang, and K. Wang, "Four sub-channel single sideband generation of vector mm-Wave based on an I/Q modulator," *IEEE Photon. J.*, vol. 11, no. 4, Aug. 2019, Art. no. 7204409.

[17] W.-J. Jiang et al., "Photonic vector signal generation employing a novel optical direct-detection in-phase/quadrature-phase upconversion," *Opt. Lett.*, vol. 35, no. 23, 2010, Art. no. 4069.

[18] H. Wang, X. Xue, S. Li, and X. Zheng, "All-optical arbitrary-point stable quadruple frequency dissemination with photonic microwave phase conjugation," *IEEE Photon. J.*, vol. 10, no. 4, Aug. 2018, Art. no. 5501508.

[19] K. Zhang, S. Li, Z. Xie, and Z. Zheng, "An all-optical Ka-band microwave long-distance dissemination system based on an optoelectronic oscillator," *IEEE Photon. J.*, vol. 14, no. 4, Aug. 2022, Art. no. 5545505.

[20] G. Qi et al., "Phase-noise analysis of optically generated millimeter-wave signals with external optical modulation techniques," *J. Lightw. Technol.*, vol. 24, no. 12, pp. 4861–4875, 2006.

[21] Y. Xu, X. Li, J. Yu, and G.-K. Chang, "Simple and reconfigured single-sideband OFDM ROF system," *Opt. Exp.*, vol. 24, no. 20, 2016, Art. no. 22830.